

3D Laser Pulse Shaping for the Cornell ERL Photoinjector

Sierra G. Cook
Physics Department, University of California, Berkeley
Berkeley, CA 94720

August 15, 2012

Abstract

The quality of the electron beam and resultant x-ray radiation produced by the proposed Energy Recovery Linear Accelerator (ERL) under development at Cornell University is limited by the quality of the electron bunch produced at the photocathode in the injector. The shape of the emitted electron bunch is determined by the shape of the laser pulse that strikes the cathode. The goal of this project is to use an adaptive optics system to shape the laser pulse and remove unwanted aberrations in the wavefront, allowing for the optimization of the electron bunch shape and improving the overall performance of the ERL.

1 Introduction and Background

The proposed energy recovery linear accelerator (ERL) currently under development at Cornell University is a new advanced synchrotron radiation source. In the ERL, electron bunches are injected into a linac and accelerated through a series of superconducting RF cavities, complete one loop around the Cornell Electron Storage Ring (CESR) emitting bright x-ray radiation, and finally, pass through the RF cavities of the linac 180 degree out of phase and are decelerated to their original injection energy. The decelerated electrons are sent to a beam dump and their energy is recycled. The photoinjector used in the ERL contains a high energy 520nm, 1.3GHz laser which strikes a photocathode and emits an electron bunch which is then accelerated through a series of superconducting RF cavities and injected into the linac. The brightness of the x-rays emitted by the ERL is largely determined by the quality of the electron pulse produced by the photocathode. The shape of the electron bunch leaving the photocathode is determined by the shape of the laser pulse, so the quality of the electron beam can be optimized by choosing a laser pulse shape that will produce a high quality, low-emittance electron pulse. However, as the laser pulse propagates to the photocathode, it acquires unwanted aberrations which alter the shape of

the wavefront and reduce the quality of the electron pulse

Project Goals:

The goals of this project were first, to correct the wavefront of the laser, eliminating any aberrations introduced by the laser's propagation through space and various optical elements between the laser and the photocathode, and secondly, to produce an arbitrary pulse shape at the photocathode. These goals can be accomplished by using an adaptive optics system to shape the wavefront of the laser pulse. The adaptive optics set-up used for this project will not be constructed or tested with the ERL laser; instead, a low-power, 532nm, non-pulsed laser will be used, and if the system is sufficiently effective, an analogous system will be employed in the ERL.

2 Relevant Theory

Fourier Optics:

An understanding of Fourier Optics is important for this project because it describes the phase propagation of light and can be used to determine how the phase of a beam changes as it propagates through space and passes through optics. The propagation of a wavefront through space is described by the equation:

$$E(x, y, z) = \frac{ik}{2\pi z} e^{ikz} e^{ik(x^2+y^2)/2z} \times \int_{-\infty}^{\infty} \int_{-\infty}^{\infty} f(\xi, \eta) e^{ik(\xi^2+\eta^2)/2z} e^{-ik((x\xi+y\eta)/z)} d\xi d\eta$$

A focusing lens adds a phase of $e^{-ik(x^2+y^2)/2f}$ to the incoming beam. If the field of the incoming beam is a constant function $E(x, y, 0) = A e^{i\psi}$ over the aperture of the lens (i.e. the beam is flat), it can be shown that if the beam propagates for one focal length after passing through the lens and picking up the additional phase, its electric field will be

$$E(x, y, f) = \frac{ik}{2\pi f} e^{ikf} e^{ik(x^2+y^2)/2f} A e^{i\psi} \delta(kx/f, ky/f)$$

In other words, if a flat-phase beam passes through a lens and propagates for one focal length, the resulting electric field will all be concentrated at the point $(x, y) = (0, 0)$.

If the field of the incoming beam at the aperture of the lens, $E(x, y)$, is not constant, the field of the beam after passing through the lens and propagating for one focal length is

$$E(x, y, f) = \frac{ik}{2\pi f} e^{ikf} e^{ik(x^2+y^2)/2f} E'(kx/f, ky/f)$$

where E' is the spatial Fourier transform of E . These results show that at the transform plane (one focal length past the lens), the intensity distribution of the beam is related to the square of the amplitude of Fourier Transform of the input beam. Therefore, changing the phase of the input beam results in an altered intensity distribution at the transform plane. This correlation between the phase of the beam and the intensity at the transform plane can be applied to the problem of 3D laser pulse shaping: by adding an appropriate phase to the input beam, an arbitrary intensity distribution can be produced at the transform plane.

Zernike Polynomials:

Zernike Polynomials are a set of polynomials commonly used in optics that are orthogonal over a unit disk. It is convenient to use these polynomials as a set of basis and to use them to describe optical aberrations. Different Zernike modes correspond to different kinds of aberrations (See figure 1), and any optical phase can be written as a weighted sum of Zernike Polynomials. Knowledge of this set of polynomials is important for this project because the software used in the adaptive optics system requires the phase of the wavefront to be input in terms of Zernike polynomials. The mathematical form of the Zernike polynomials is shown below:

Even polynomials:

$$Z_n^m(\rho, \varphi) = R_n^m(\rho) \cos(m \varphi)$$

Odd Polynomials:

$$Z_n^{-m}(\rho, \varphi) = R_n^m(\rho) \sin(m \varphi)$$

where

$$R_n^m(\rho) = \sum_{k=0}^{(n-m)/2} \frac{(-1)^k (n-k)!}{k!((n+m)/2-k)!((n-m)/2-k)!} \rho^{n-2k}$$

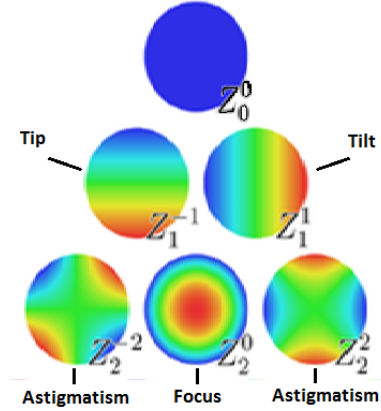


Figure 1: Zernike Modes [1]

3 Experimental Methods

The adaptive optics system used in this experiment was a commercially available system manufactured by Okotech. The system includes three components: a wavefront sensor, a deformable mirror, and Frontsurfer adaptive optics software.

Wavefront Sensor

The wavefront sensor (WFS) operates on the same principle as a Shack-Hartmann sensor. The incoming beam passes through an array of lenslets and is focused onto a sensor. If the incoming beam is collimated the wavefront is flat, and therefore it will pass directly through the lenslet array and focus to a point on the sensor directly behind each lenslet. However, if the wavefront is not flat, it will pass through the lenslets in the array at different angles and the points of focus on the sensor will be shifted. By analyzing the direction and amount by which each spot is shifted on the sensor from the flat-wave pattern, the phase of the wavefront can be reconstructed. A schematic of a Shack-Hartmann sensor is shown in figure 2. The wavefront sensor used in this project contained a lenslet array of 127 microlenses arranged in a 3.9mm hexagonal grid; in order to reconstruct the wavefront, the pattern formed on the sensor by the incoming beamed is compared to an ideal hexagonal grid.

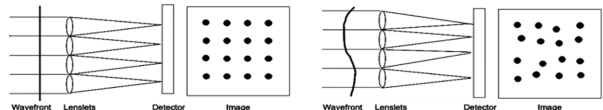


Figure 2: Shack-Hartmann Sensor [7]

Deformable Mirror

An OKOTech micromachined membrane deformable mirror (MMDM) with a 37-channel, 12mm hexagonal actuator structure and a 15mm aperture was used. A picture and schematic of the MMDM are shown in figure 3.

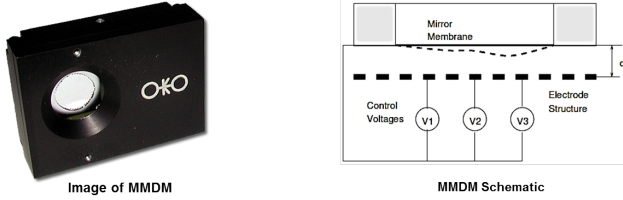


Figure 3: Micromachined Membrane Deformable Mirror [10]

Applying voltage to the actuators deforms the mirror by applying an attractive force on the membrane, pulling it towards the actuator. The deformable mirror is used to change the phase of the incoming laser beam, and the shape of the added phase corresponds directly to the shape of the mirror deformation. By applying the appropriate voltages to the mirror actuators, the mirror membrane can be deformed into virtually any shape, and an arbitrary phase can be produced. A simplified illustration of the correlation between mirror deformation and the shape of the resulting phase is shown in figure 4.

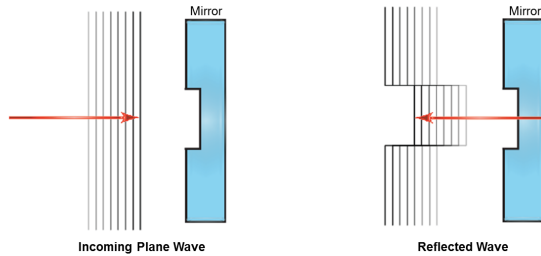


Figure 4: The deformation of the mirror causes parts of the incoming waves to travel farther than others before reflection, causing a direct correlation between the deformation shape and the phase shape of the reflected beam.

Frontsurfer Software

The software used consolidates the system, taking in data from the wavefront sensor, analyzing it, and applying voltages to the mirror actuators accordingly until the desired wavefront shape is achieved.

Interfacing with the Wavefront Sensor:

The Frontsurfer software superimposes an ideal hexagonal reference grid onto the image of the spot pattern of the

beam passing through the WFS lenselet array, and reconstructs the wavefront by analyzing the difference between the reference and experimental hexagonal spot patterns.

Interfacing with the MMDM:

The voltage of each of the 37 MMDM actuators can be set manually or a target function can be entered into the software as a weighted sum of Zernike polynomials, with the Zernike amplitudes input in microns. The software will begin a feedback loop, intaking data from the WFS and adjusting the MMDM actuator voltages accordingly until the target function is produced. If the aberration ϕ_n remaining after the n^{th} iteration corresponds to the set of actuator signals X_n , then the actuator signal X_{n+1} at the next iteration is described by the equation:

$$\mathbf{X}_{n+1} = \mathbf{X}_n - g\mathbf{A}^{-1}\phi_n$$

where g is the feedback coefficient which is always in the range $(0...1]$, \mathbf{A} is the influence matrix of the mirror, and the pseudo-inverse of \mathbf{A} is found by singular value decomposition:

$$\mathbf{A}^{-1} = \mathbf{V}\mathbf{S}^{-1}\mathbf{U}^T$$

\mathbf{U} , \mathbf{S} , and \mathbf{V} are the singular value decomposition of

$$\mathbf{A} = \mathbf{U}\mathbf{S}\mathbf{V}^T$$

The columns of \mathbf{U} comprise an orthonormal set of mirror deformations, and the element of the diagonal matrix \mathbf{S} are the "singular values" or gains of these modes

It is important to calibrate the mirror before running feedback whenever the experimental set-up has been adjusted; calibration applies voltage to each of the actuators sequentially, measures the response of the wavefront, and calculates the singular values.

While in this project the MMDM was used to correct static aberrations and to add constant phases to the beam, the software provides feedback and runs continuous iterations to allow for the correction of dynamic aberrations.

Other Key Features:

Singular Values: Frontsurfer software displays the number of active modes of the mirror. Which modes are active and which are not is determined by setting a threshold on the singular values corresponding to each mode (in this case, singular values >0.01 were classified as active; the value of the threshold is adjustable in the Frontsurfer software). The number of active modes is a good indicator of whether or not the incoming beam is the correct size. If

the beam is too small, there will be fewer active modes because the beam will not cover the entire surface of the actuator structure, so movement to peripheral actuators will not be able to produce the desired effect on the shape of the beam. Thus, if the program is failing to generate target phases effectively, a check of the number of active modes of the mirror can help identify the cause of the error.

Final Report: After running feedback to generate a target function, a final report of the Zernike polynomials comprising the generated wavefront is produced. This report describes the final phase of the wavefront in terms of Zernike modes, listing the coefficient of each mode and highlighting the dominant component. Graphing this data and comparing it to a graph of the target function provides a simple way to determine how successfully the software reproduced the target function.

Feedback Loop: The software can run a continuous feedback loop displaying a bar graph indicating the weight of various low-order aberrations, including defocus, astigmatism, and coma; this allows the user to instantaneously observe the effects of adjustments to the optical system. This feature is especially useful when trying to reduce aberrations introduced by imprecise alignment of optical components. However, it is important to recall that the MMDM must be recalibrated after every adjustment of the experimental set-up so it is best to use a flat mirror rather than the MMDM when using the feedback loop for alignment purposes, or alternatively, to make adjustments in small increments and recalibrate the MMDM often throughout the process.

Additional Data: In addition to a reconstruction of the wavefront, Frontsurfer software generates an interferogram, and an image of the far-field intensity distribution. The interferogram proved helpful in determining whether the mirror was successfully generating target functions by comparing the interferograms produced by various Zernike aberrations to those shown in the technical passport of the MMDM used.

An image of the various data types produced by the Frontsurfer software is shown in figure 5.

4 Experimental Process and Results

Goal 1: Cleaning Up the Laser Beam

The first goal of this project was to remove any unwanted aberrations in the wavefront and to return the wavefront to a flat-phase wave. The initial experimental set-up is shown in figure 6.

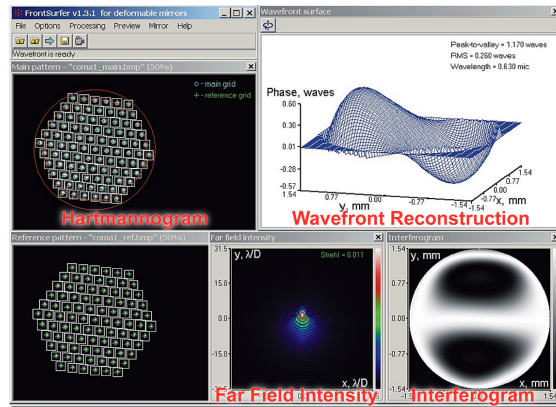


Figure 5: Frontsurfer Software Interface: Clockwise from Top Left: (1) Hartmannogram, (2) Wavefront Reconstruction, (3) Interferogram, (4) Far-Field Intensity Distribution (5) Beam on Wavefront Sensor

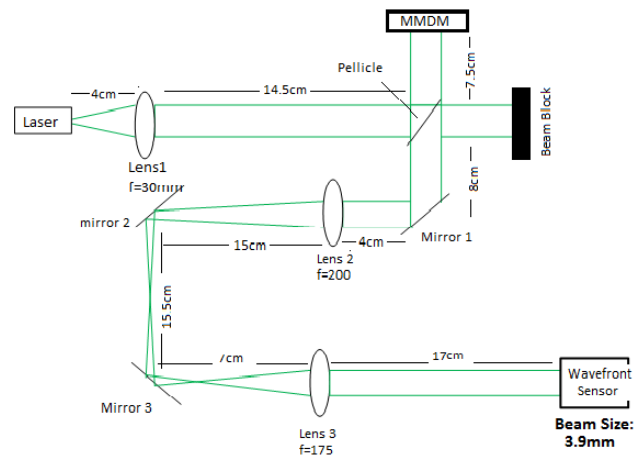


Figure 6: Initial Experimental Set-Up

Using this set-up, it was possible to generate certain low-order Zernike polynomial target functions (specifically, astigmatism Z_2^{-2} and defocus Z_2^0); however, the interferograms for higher Zernike polynomials did not agree well with those shown in the technical passport of the MMDM used. At its best, the system was capable of producing a flat-phase wavefront with a peak-to-valley distance of 0.25 waves; while this was a promising initial result, a flatness of 0.1 wave was desired. An image of a flattened wavefront produced with this experimental set-up is shown in figure 7.

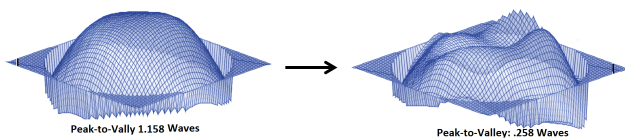


Figure 7: Results from Initial Set-Up

Although the system was able to flatten waves somewhat effectively, its inability to produce waves with a peak-to-valley distance less than 0.25 waves or to generate higher-order Zernike terms imposed severe limits on the usefulness of the system. To determine the source of the non-flatness in the final wavefront, the WFS was used to determine the flatness of the beam at various points along the beam path. It was measured directly after collimation, directly after passing through the pellicle, in the MMDM plane, and in the plane of lens 2. At all points, the peak-to-valley distance was between 0.215 and 0.250 waves, and adjustments in the set-up only decreased the flatness.

One potential explanation for the non-flatness of the wavefront was the size of the beam. It was realized that only 18 (out of 37 possible) modes of the mirror were active. The beam was measured using a CCD camera and found to be 4mm, which was an appropriate size for the 3.9mm wavefront sensor, but too small for the 12mm actuator structure of the MMDM. The beam was expanded at the MMDM and then resized so it would not be too large for the wavefront sensor. A schematic of the new set-up is shown in figure 8.

With the new set-up, 31 modes of the MMDM were active and the performance of the system improved dramatically. The Zernike aberrations demonstrated in the MMDM technical passport were input as target functions and the generated wavefront and interferograms matched those shown in the passport adequately (the lower orders matched almost perfectly).

The system was also able to repeatedly generate waves with a peak-to-valley distance of less than 0.1 waves. This indicates that the system is in fact an effective mechanism for removing any unwanted aberrations that alter the wavefront from its original flat phase. An image of the system

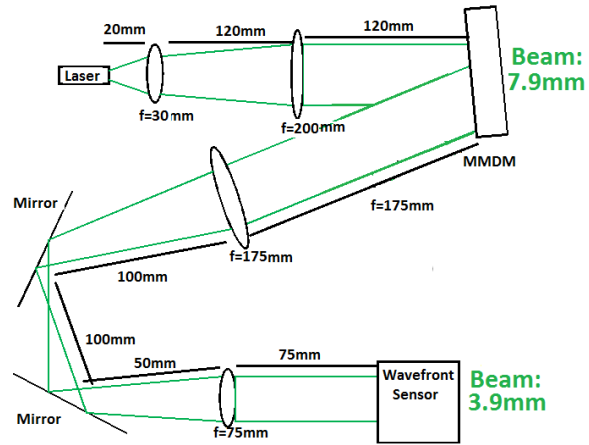


Figure 8: Experimental Set-Up with Resized Beam

flattening a wavefront is shown in figure 9.

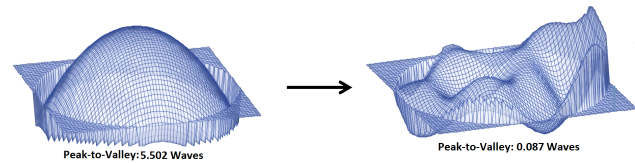


Figure 9: Result from Improved Set-Up

Shaping the Laser Pulse

The second goal of this project was to produce a laser beam with an arbitrary shape by using the MMDM to add an appropriate phase passing the beam through a Fourier transforming lens. As previously stated, the intensity distribution of the resultant image on the focal plane is related to the square of the Fourier transform of the input beam. A focusing lens and a CCD camera were inserted into the system. The function of the focusing lens was to take the Fourier transform of the beam, and the CCD was placed in the transform plane (where the photocathode would be positioned in the ERL) to observe the intensity distribution. A schematic of this set-up is shown in figure 10

As a first step to determining whether this adaptive optics system could be used to produce a beam of arbitrary shape, an attempt to transform a Gaussian beam into a flat-top was made.

Transforming a Gaussian Beam into a Flat-Top:

First, the phase needed to transform a Gaussian into a flat-top beam must be calculated, a shown below:

The calculation to determine the phase is carried out in three steps. The calculations consider an incoming beam from $z = -\infty$, passes through a lens and beam-shaping

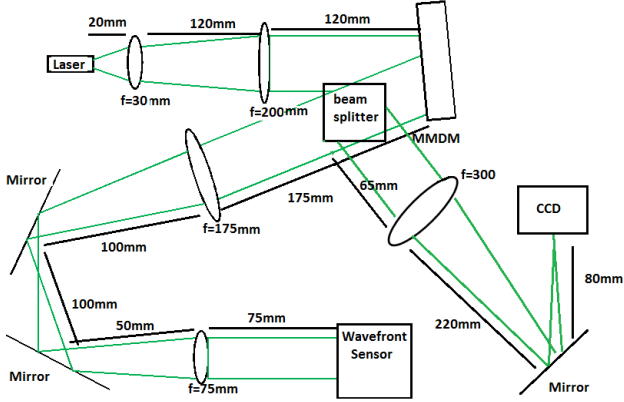


Figure 10: Experimental Set-Up with CCD

element, and propagating to $z = f$.

1) Determine the constant A that defines the intensity of the output beam by requiring that the energy of the incoming and outgoing beams are the same:

$$E_{in} = \int_{-\infty}^{\infty} I(s/R) ds = R \int_{-\infty}^{\infty} I(s) ds$$

$$E_{out} = \frac{AR}{D} \int_{-\infty}^{\infty} Q(s/D) ds = AR \int_{-\infty}^{\infty} Q(s) ds$$

$$A = \frac{\int_{-\infty}^{\infty} I(s) ds}{\int_{-\infty}^{\infty} Q(s) ds}$$

In the case of a radial gaussian beam,

$$Q = 1; s < 1$$

$$Q = 0; s > 1$$

Using these restrictions on Q to solve for A :

$$A = \frac{1}{2\pi}$$

2) The second step is to describe a function that maps rays at the plane of the phase-adding optical element (in this case an MMDM) to rays at the focal plane. More specifically, a function that maps rays at the lateral position $x = R\xi$ at the MMDM to rays at the position $x = D\alpha(\xi)$ at the focal plane. This is done by asserting that a bundle of rays at the MMDM plane has the same energy as the same bundle of rays in the focal plane. Mathematically, this condition is represented by the following equation:

$$\int_{-\infty}^{\xi} I(s) ds = A \int_{\alpha(\xi)}^{\infty} Q(s) ds$$

While $\alpha(\xi)$ is defined by this equation, it will prove more convenient to instead consider its derivative:

$$AQ(\alpha) \frac{d\alpha}{d\xi} = -I(\xi)$$

For the case of converting a Gaussian to a flat-top beam,

$$\alpha(\xi) = \sqrt{2\pi} \sqrt{1 - e^{-\xi^2}}$$

3) The third step is to calculate the function $\phi(\xi)$ that describes the phase shift introduced by the deformable mirror. This is done by determining the time it takes for a ray to travel from its source, reflect off of the MMDM and pass through the focusing lens, and propagate to the focal plane. The travel time can be broken down into three parts: the time to travel from the source $(0, -L)$ to a point on the MMDM $(R\xi, 0)$, the time delay introduced as the beam encounters the MMDM at $(R\xi, 0)$, and the time for the beam to travel from $(R\xi, 0)$ on the MMDM to a point $(D\alpha, f)$ at the focal plane.

The total time traveled is

$$t(\xi, \alpha) = t_L(\xi) + t_{delay}(\xi) + t_f(\xi, \alpha)$$

$$t(\xi, \alpha) = \frac{1}{c} \left(L + \frac{\xi^2}{2L} \right) - \xi^2 \frac{R^2}{2fc} + \phi(\xi) \frac{RD}{fc} + \frac{f}{c} + \frac{(D\alpha - R\xi)^2}{2fc}$$

To be consistent with Fermat's principle, the travel time of the beam must be stationary with respect to a beam that starts from $(0, -L)$, reaches the MMDM at a point $(R\xi + Rd\xi, 0)$, and travels directly to $(D\alpha, f)$ in the focal plane. Therefore the travel time must satisfy the condition

$$\frac{\partial t(\xi, \alpha)}{\partial \xi} = 0$$

simplifying $\partial/\partial\xi(t_L + t_{delay} + t_f)$ yields the simple equation:

$$\frac{d\phi}{d\xi} = \alpha(\xi)$$

Which can easily be solved for $\alpha(\xi)$

$$\alpha(\xi) = \sqrt{2\pi} \sqrt{1 - e^{-\xi^2}}$$

Solving the differential shown above for $\phi(\xi)$ yields the phase for converting a Gaussian to a flat-top beam:

$$\phi(\xi) = \sqrt{2\pi} \int_0^{\xi} \sqrt{1 - e^{-s^2}} ds$$

Because the beam passes through a Fourier transforming lens after being reflected by the MMDM, the additional phase of $e^{-ik(x^2+y^2)/2f}$ added by the lens must be also be taken into account and compensated for. Therefore, the total phase that must be added to the beam by the MMDM is:

$$\phi(\xi) = \frac{D_{final}k}{2f} \int_0^{\xi} \sqrt{1 - e^{-s^2}} ds$$

Once the phase has been calculated, it is necessary to write it as a weighted sum of Zernike polynomials so the

phase can be input into the Frontsurfer software. This calculation takes advantage of the orthogonality of Zernike polynomials, as shown below:

$$\begin{aligned} \phi(r) &= \sum Z_{mn}(r, \phi) A_{mn} \\ \langle \phi(r) | Z_{pq} \rangle &= \sum \langle Z_{mn} | Z_{pq} \rangle A_{mn} \\ &= \langle \phi(r) | \delta_{mp} \delta_{nq} A_{mn} \\ A_{mn} &= \langle \phi(r) | Z_{mn} \rangle \end{aligned}$$

The Zernike coefficients were calculated using Mathematica and are shown in figure 11.

Zernike Mode [n,m]	Coefficient
[0,0]	14.1577
[2,0]	7.089
[4,0]	-0.703
[6,0]	0.099
[8,0]	-0.013

Figure 11: Zernike Coefficients to Transform a Gaussian Beam into a Flat-Top

The calculated coefficients were input as the target function in the Frontsurfer software; the intensity profile of the beam measured by the CCD compared to the results of a MATLAB simulation of converting a Gaussian to a flat-top is shown in figure 12. The MATLAB code, written by Adam Bartnik, mathematically propagated the beam according to Fourier optics (due to the symmetric nature of the problem, Hankel transforms were used instead of Fourier transforms) through the experimental set-up, adding the appropriate phase at the MMDM plane, and measuring the intensity distribution at the transform plane.

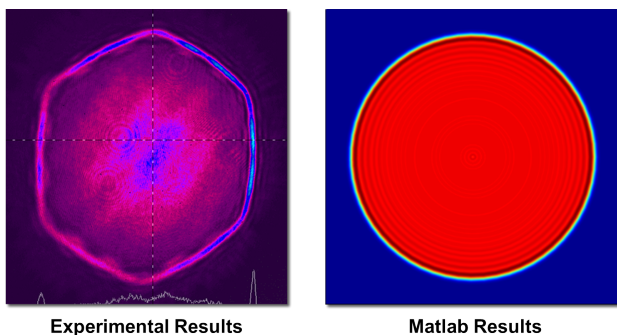
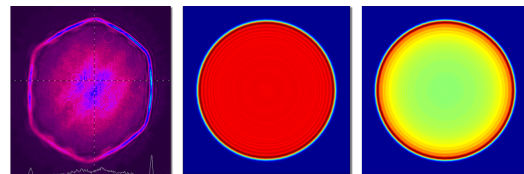


Figure 12: Comparison Between Experimental and Simulated Flat-Top Beams

Notable features of the experimental results are the hexagonal shape of the beam and the bright fringes.

The actuator structure of the MMDM is hexagonal, so the shape of the beam can be attributed to the mirror, although the exact cause is less obvious. An incorrect initial beam size was proposed as a potential cause for the unusual features of the beam. Figure 13 shows a comparison between the experimental results and the results of the simulation when the initial size of the beam was 10 percent larger, and 10 percent smaller, respectively, than the initial beam size used to calculate phase.



Experimental Results 10% Too Large 10% Too Small

Figure 13: Comparison between experimentally derived "flat-top" and simulation results for an incorrect initial beam size

It can be seen that the matlab simulations also exhibit different intensities around the edges, possibly explaining the bright fringes on the experimental results, but failing to explain the hexagonal edges observed in the experimental intensity distribution.

Clipping of the beam on the edge of the actuator structure was proposed as an explanation for the hexagonal intensity distribution. To test this idea, the beam size was reduced from 7.9mm to 5mm at the MMDM. An image of the resultant intensity distribution is shown in figure 14.

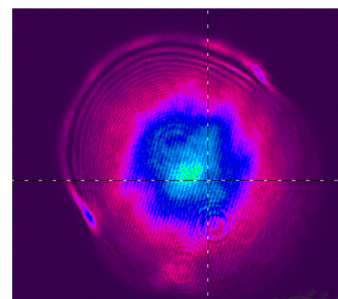


Figure 14: Intensity Profile of 5mm at CCD Plane

While this eliminated the hexagonal shape of the beam, strange edge behavior was still apparent and the beam was not a flat-top. Other target functions were input, and it was found that the system could not generate even low order Zernike polynomials. The mirror was found to have only 19 active modes, which explained the systems failure to produce target functions and indicating that the beam was too small. The beam was increased to 5.75mm, and the

resultant intensity distribution is shown in figure 15.

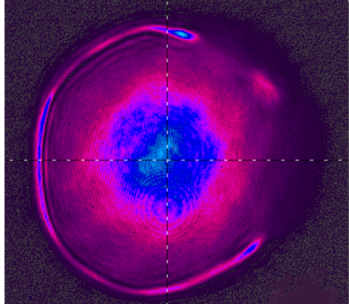


Figure 15: Intensity Distribution of 5.75mm at CCD Plane

The number of active modes of the MMDM was 28 and the system was able to generate low order Zernike polynomials, but higher orders could not be produced. The intensity distribution, while slightly improved from the result of the 5mm beam, still exhibited bright fringes and was not flat. From these results it became apparent that systems failure to produce a flat-top beam was not due solely to the incorrect sizing of the beam.

It was found that when the calculated flat-top Zernike coefficients were input as the target function, it maxed out the voltage applied to the actuators of the MMDM, which could explain the systems inability to produce a flat-top beam. One proposed solution to this problem is to reduce the magnitude of the phase, consequently reducing the coefficients of the Zernike polynomials so they could be input into the software without maxing out the actuator voltages. As shown previously, the phase added by the MMDM is

$$\phi(\xi) = \frac{D_{final}k}{2f} \int_0^\xi \sqrt{1 - e^{-s^2}} ds$$

The magnitude of the phase can be reduced by increasing the size of the initial beam. However, when a beam size of 10mm (the largest beam size that could reasonably be used without clipping on the MMDM actuator structure) was used to recalculate the Zernike coefficients, they were still too large to input as a target function in the software without maxing out the actuator voltages. Retrospectively, it can be seen that the Zernike coefficients should have been recalculated when the beam was resized to 5mm and 5.75 mm because the phase ϕ depends on w , the initial beam width. However, inputting the reduced beam size into the calculations would have yielded even higher magnitude coefficients of the Zernike polynomials, so the undesirable beam behavior exhibited in those tests cannot be attributed to the failure to recalculate the Zernike polynomials.

Although reducing the phase by altering the initial beam width proved impossible, other ways to reduce the phase may still be effective. Using a Fourier transforming lens with a longer focal length, and positioning the CCD in the

focal plane of the new lens would also decrease the phase. Replacing the Fourier transforming lens would be simple and convenient, and is a logical next step to take in this project.

5 Conclusions

It was shown that the adaptive optics system employed can effectively remove aberrations in flat wavefront, successfully flattening the beam to within 0.1 wave. While the goal of producing an arbitrary beam shape was not completed, significant progress was made, potential sources of the problems encountered were investigated, and possible solutions and steps for the future continuation of this project were proposed.

References

- [1] Adaptive Optics Guide. *OKO Flexible Optical Manual* April 2008 Edition.
- [2] Adaptive Optic Systems. *OKOtech Flexible Optical*. <<http://www.okotech.com/ao-systems>>
- [3] Dickey, Fred; Holswade, Scott. *Laser Beam Shaping: Theory and Techniques*. Copyright 2000, Marcel Dekker, inc.
- [4] Dunham, et al. *University ERL Injector* erl.chess.cornell.edu/papers/2008/FirstTestoftheCornellUniversityERL
- [5] Flexible Optical B.V. *FrontSurfer Wavefront Analysis and Control System*. OKO Technologies
- [6] Maeda Y. Patrick *Zernike Polynomials and Their Use in Describing the Wavefront Aberrations of the Human Eye*. Applied Vision and Imaging Systems. <<http://scien.stanford.edu/pages/labsite/2003/psych221/projects/03/pmaeda/index.html>>
- [7] Vallerga, John et al. *Optically Sensitive Medipix2 Detector for Adaptive Optics Wavefront Sensing*. ScienceDirect.com
- [8] Wavefront Sensors. *OKO Flexible Optical*. <<http://www.okotech.com/sensors>>
- [9] Wavefront Sensors: Shack-Hartmann <<http://www.ctio.noao.edu/atokovin/tutorial/part3/wfs.html>>
- [10] 15mm 37-Ch "OKO Mirror". *OKO Flexible Optical*. <<http://www.okotech.com/15-mm-37-ch-qoko-mirrorq>>